

PooDLe🐶: Pooled and dense self-supervised learning from naturalistic videos

Alex N. Wang^{*,1}, Christopher Hoang^{*,1}, Yuwen Xiong, Yann LeCun^{1,2}, and Mengye Ren¹

¹New York University ²Meta *Equal Contribution

Correspondence to: {anw2067, ch3451, mengye}@nyu.edu

Project page: poodle-ssl.github.io

Abstract

Self-supervised learning has driven significant progress in learning from single-subject, *iconic* images. However, there are still unanswered questions about the use of minimally-curated, naturalistic video data, which contain *dense* scenes with many independent objects, imbalanced class distributions, and varying object sizes. In this paper, we propose a novel approach that combines an invariance-based SSL objective on pooled representations with a dense SSL objective that enforces equivariance to optical flow warping. Our findings indicate that a unified objective applied at multiple feature scales is essential for learning effective image representations from high-resolution, naturalistic videos. We validate our approach on the BDD100K driving video dataset and the Walking Tours first-person video dataset, demonstrating its ability to capture spatial understanding from a dense objective and semantic understanding via a pooled representation objective.

1 Introduction

Humans and other animals learn visual understanding from a continuous stream of inputs with little explicit supervision. Recently, self-supervised learning (SSL) [2–4, 7, 11, 12, 20, 25, 26] has made great strides in learning without human annotations, becoming competitive with supervised learning. However, most methods still revolve around ImageNet [15] which is implicitly supervised through *iconic* images that contain an unambiguous subject sampled from a balanced class distribution. In contrast, naturalistic vision data such as egocentric videos, contain cluttered scenes, imbalanced classes and objects of varying size, making them ill-suited for existing iconic methods.

Nevertheless, these naturalistic videos are still valuable for their information density and ease of collection, while also mimicking the real-life perspective of humans. Unfortunately, the aforementioned iconic methods, which learn to align pooled representations of an image, may perform poorly as dense scenes often produce views depicting unrelated subjects that are semantically incompatible (Figure 1b, red boxes). Recent works have attempted to address this weakness by introducing mechanisms to account for multiple subjects, such as new cropping [39] or attention [35, 42] strategies. Others [45, 49] have also proposed variations using a “dense SSL” objective, which does not pool image representations and instead identifies correspondences between views before computing an SSL loss for each corresponding region.

While dense SSL methods avoid the problem of aligning semantically incompatible views, and can learn fine-grained object boundaries [49], they are susceptible to other issues. Computing the loss at each spatial location presents a spatial imbalance problem, where larger background classes such as the sky dominate the representation while smaller classes such as pedestrians are underrepresented. This effect is undesirable because foreground objects, which are often smaller, should be favored over low-detail, repetitive background classes which often occupy more space. Furthermore, ignoring small foreground objects can be acutely hazardous in applications like self-driving [50] where critical objects, such as traffic lights and pedestrians occupy less than 0.3% of a video frame (Figure 1b, green boxes and 1c). Preserving these crucial details is particularly necessary in the SSL, where there are no labels to assign importance. This is in contrast to ImageNet [15] training, where models that can easily learn semantics from iconic data with clear, single-subject

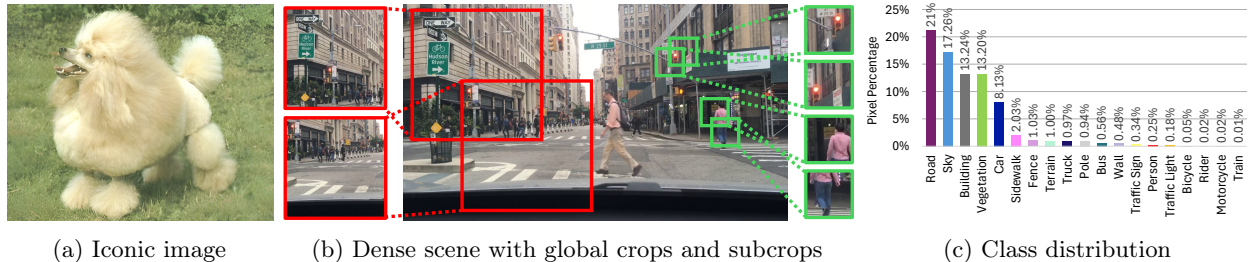


Figure 1: *Challenges of SSL on dense, naturalistic video* include training on crowded scenes with many objects of varying scale and class imbalance. (a) Iconic image from ImageNet [15]. (b) Dense scene from BDD100K [50]. Global crops (red boxes) typically used in iconic methods may contain disjoint sets of subjects and multiple subjects per crop. Subcrops (green boxes) can provide pseudo-iconic views of a single subject. (c) Long-tailed distribution of classes, by percentage of pixels, from the BDD100K semantic segmentation benchmark. The example subcrops show smaller object classes such as "Traffic Light" and "Person."

views and a balanced class distribution. Some dense SSL methods [35, 42, 45] also include losses that optimize a global, pooled representation to learn semantic information from dense scenes, but do not explore how to integrate these two objectives through means of architecture and augmentation strategies.

To address problems of cluttered scenes and spatial imbalance when learning from dense, naturalistic videos, we propose a joint **Pooled** and **Dense Learning** (PooDLe) method that optimizes a dense SSL objective over representations without pooling and a secondary pooled objective applied to smaller, content-aligned views. The combination of dense and pooled objectives captures both scene-level understanding and fine-grained boundaries, as well as high-level semantics and small objects. Like FlowE [49], our dense objective encourages the alignment of dense feature maps using optical flow warping. We also use a flow-informed cropping procedure to generate pairs of smaller views, or "subcrops", with improved subject correspondence between each subcrop pair when training the pooled loss. Depicted in Figure 1, these subcrops often serve as pseudo-iconic views of foreground objects, which functionally increase the prevalence of smaller foreground classes in our dataset. We also introduce a lightweight spatial decoder module (SDM), comprised of top-down decoder layers and UNet [38]-like lateral connections to upsample high-level semantic representations to preserve smaller objects in our dense objective. We find the inclusion of both objectives along with the SDM is essential to capture the semantics of smaller objects and to achieve overall strong downstream task performance.

We conduct experiments on the BDD100K [50] dataset of dashcam driving videos and the recent WalkingTours dataset of first-person walking videos [42]. PooDLe achieves state-of-the-art performance on downstream semantic segmentation and object detection benchmarks, with a notable gain on recognizing small objects. In our ablations, we demonstrate that our joint objective formulation and the SDM are critical for success. In addition, our approach maintains strong performance over a wide range of crop areas and input resolutions while the pooled or dense objective alone quickly degrades

In summary, our contributions are as follows:

1. We introduce PooDLe, a method combining a dense SSL objective based on flow equivariance and a pooled objective using small pseudo-iconic subcrops. PooDLe unifies the two objectives with a spatial decoder module to combine the strengths of both objectives.
2. When pretrained on naturalistic videos, PooDLe achieves state-of-the-art downstream performance on BDD100K [50], ADE20K [53] and Cityscapes [14] semantic segmentation, and BDD100K object detection tasks. PooDLe outperforms prior dense SSL methods [45, 49], particularly on small objects, and is competitive with ImageNet pretraining.
3. We study the effects of crop area, resolution and temporal stride between paired frames. We demonstrate the importance of maintaining pixel density when increasing image resolution for the dense SSL objective. We also perform analysis to show that subcrops can increase prevalence of small objects in the pooled objective by serving as pseudo-iconic views, which supports our experimental findings.

2 Related Work

Self-supervised learning with iconic images. Representation learning on iconic image datasets has a long history from denoising autoencoders [43] to joint embedding methods [3, 7, 11, 20, 25, 51] to joint-embedding predictive architectures [2, 5]. Joint embedding methods learn representation invariance to visual changes created by augmentations using contrastive [11, 33], mean squared error [20], or classification [6, 7] losses between corresponding pairs, pushing SSL to new heights on ImageNet classification. Later works have extended these methods to internet-scale data [34] and included other modalities like text [37]. Separately, the MAE [26] family of methods learn via reconstruction of masked image regions. iBOT [54] combines joint embedding methods with token reconstruction to produce impressive results on ImageNet classification. [6, 7, 34, 54] all generate small, low-resolution crops (‘multi-crop’) that are optimized to predict the representations of global crops for iconic training examples for little additional compute. This is different from our subcrop strategy which produces aligned image pairs of small crops as pseudo-iconic views from otherwise dense scenes.

Training using dense multi-subject images. Following the success of SSL on ImageNet, other works seek to learn from dense, multi-subject images where augmented views may not contain corresponding subjects for invariance learning. [8, 45, 48] build upon joint-embedding methods, relying on similarity of features bootstrapped from typical invariance learning to identify positive pairs across dense, unpooled feature maps. [27, 44] optimize dense losses, contrasting pixels belonging to different semantic classes; these methods require off-the-shelf segmentation modules. [21, 55] utilize DINO [7] attention maps to identify training pairs, while ADCLR [52] identifies pairs using small ‘query’ crops and the patches that attend to them. All of these methods make strides towards learning from dense images with multiple objects. However, these methods do not consider the effects of a dense objective on per-class accuracy and the skewed class and spatial distributions of more naturalistic data.

Learning image representations from video data. Extending beyond images, other works have sought to capture the variance of objects through time by training on pairs of video frames. Gordon et al. [19] adapts contrastive learning to use correlated frames as positive examples, while [29, 35] identify positive pairs using high representational similarity. FlowE [49] builds on BYOL [20] and identifies positive spatial regions between frames using off-the-shelf flow. Most recently, DoRA [42] proposes a new dense video dataset and extends DINO by clustering over many frames to identify and track objects for representation learning. In the MAE paradigm, [17, 41] directly reconstruct sequences of frames while [22, 46] perform reconstruction given a corresponding overlapping frame. MC-JEPA [5] learns motion using video data by aligning latent representations throughout the feature pyramid while performing representation learning on ImageNet while VJEPA [4] directly aims to learn video representations via latent video prediction. Like some methods above, PooDLe learns a rich image representation from video data and does so using a dense and pooled objective to capture both scene-level spatial understanding and high-level semantics.

3 PooDLe: Pooled and Dense Learning from naturalistic videos

We present PooDLe, a self-supervised method for learning dense visual representations using paired frames from naturalistic, first-person videos. PooDLe combines two SSL objectives: a *dense* objective for learning representations of dense, crowded scenes; and a *pooled* objective on small subcrops sampled using flow-aware cropping augmentations. We also propose a lightweight spatial decoder module (SDM) that uses top-down decoder layers and UNet-like *lateral* connections to earlier encoder representations to both upsample the high-level representations and resurface fine-grained details and small objects that may get lost in downsampling operations. For a high-level overview of PooDLe, see Figure 2.

Preliminaries. Inputs to the model are video frame pairs $\mathbf{x}_t, \mathbf{x}_{t+\Delta t}$ with dimensions $H \times W$, and dense optical flow $M_{t \rightarrow t+\Delta t}$ predicted by an external optical flow model. Randomly sampled augmentations A_1 and A_2 are applied to each example to create positive training pairs. In a similar setup to BYOL, the encoder and projector are denoted as a function $\mathbf{p} = f(\mathbf{x})$ using either online weights θ or offline, EMA-updated weights ξ . The predictor module $q_\theta(\cdot)$ only has online weights θ . Separate projector and predictor modules are used for the pooled and dense objectives, but are not annotated for simplicity. We use a ResNet-50 backbone, as well as projectors and predictors following FlowE [49] and BYOL [20], that are discarded after pre-training.

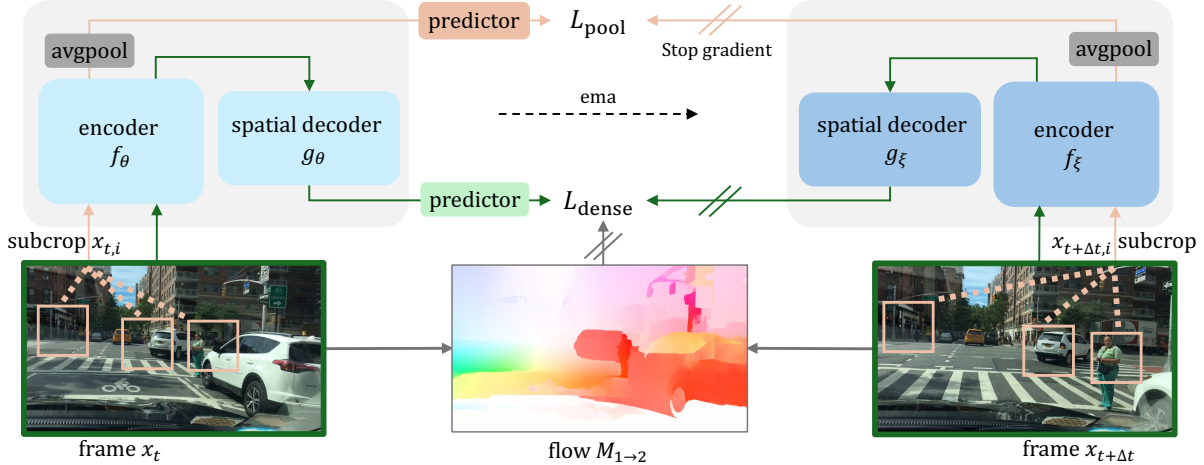


Figure 2: PooDLe combines pooled and dense learning objective for video self-supervised learning. **Green** path: dense objective performing flow-equivariance learning on the output of the decoder $g(\cdot)$. **Orange** path: pooled objective encoding K subcrops sampled with flow-informed local cropping. Projector modules are omitted for simplicity. Offline parameter ξ are the exponential moving average (ema) of online parameters θ .

Dense SSL with flow equivariance. The dense objective follows FlowE [49] by using optical flow $M_{t \rightarrow t+\Delta t}$ to align paired feature projections \mathbf{p}_t and $\mathbf{p}_{t+\Delta t}$. At a high-level, this objective minimizes differences in representation between corresponding regions. More specifically, the inverse augmentation functions A^{-1} and optical flow are used to align the representations \mathbf{p} and after upsampling to input resolution $H \times W$, the objective is the squared error:

$$\mathcal{L}_{\text{dense}} = \frac{1}{HW} \left\| q_\theta(A_1^{-1}(\mathbf{p}_t)) - (M_{t \rightarrow t+\Delta t} \circ A_2^{-1})(\mathbf{p}_{t+\Delta t}) \right\|_2^2, \quad (1)$$

where normalization is applied after the predictor and flow warping.

Pooled objective with flow-informed subcrops. First we identify K pseudo-iconic subcrop pairs. Unlike for iconic data, random crops from paired frames are unlikely to contain a common subject. To mitigate this, we once again use optical flow in a *flow-informed* cropping procedure to identify aligned training pairs. For each subcrop pair, we sample a random point (u, v) in the target frame $\mathbf{x}_{t+\Delta t}$ to serve as the crop center. It is then warped into the earlier frame \mathbf{x}_t using flow $M_{t \rightarrow t+\Delta t}$ plus random jitter (δ_u, δ_t) for paired center (u', v') . A crop is made around each center, with an area sampled from $U[s_{\min}, s_{\max}]$ of the global crop for subcrops $\mathbf{x}_{t,i}$ and $\mathbf{x}_{t+\Delta t,i}$.

As we require both crop centers to land within the bounds of the image, subcrops tend to be center-biased [36] and lack diversity. To remedy this, we employ a grid-sampling procedure for selecting the initial crop center (u, v) . Each global crop \mathbf{x} is divided into a grid with cells of side length $d_{\text{grid}} = \min(H, W) \times \sqrt{(s_{\min} + s_{\max})/2}$ for a $H/d_{\text{grid}} \times W/d_{\text{grid}}$ grid. Each cell is selected without replacement and a center (u, v) is then uniformly sampled within the cell.

After K pairs $(x_{t,k}, x_{t+\Delta t,k})$ are generated, they are encoded via the backbone and the pooled objective projector. Unlike in the dense objective, no alignment or upsampling is performed, and each projection \mathbf{p} is averaged-pooled over its spatial dimensions before computing the loss:

$$\mathcal{L}_{\text{pool}} = \frac{1}{K} \sum_k \left\| q_\theta(\bar{\mathbf{p}}_{t,k}) - \bar{\mathbf{p}}_{t+\Delta t,k} \right\|_2^2, \quad (2)$$

where $\bar{\cdot}$ denotes average pooling over spatial dimensions with normalization performed after. Our approach trains each subcrop to predict its corresponding pair, likely containing the same objects in dense scenes. This differs from multi-crop [6], which has local crops predict global crops — potentially less effective for dense scenes where local crops may only capture a subset of objects.

Spatial Decoder Module (SDM). We introduce SDM (Figure 3b) to both upsample high-level encoder features and preserve information from lower layers, particularly any smaller foreground objects that may be lost due to pooling operations. Its design draws inspiration from convolutional UNet [38] and FPN [31] and improves upon FlowE’s use of dilated convolutions to replace pooling by efficiently maintaining high-resolution representations while significantly reducing activations and memory usage.

The SDM utilizes decoder blocks, each consisting of an *upsample* operation, a computation block of processing layers $g(\cdot)$, and a UNet-like *lateral* connection. The output of each block is computed as:

$$\mathbf{z}^{l+1} = g(\text{upsample}(\mathbf{z}^{(l)})) + \text{lateral}(\mathbf{z}^j), \quad (3)$$

where $\mathbf{z}^{(l)}$ is the representation after the l^{th} encoder stage and $\mathbf{z}^{(j)}$ is an earlier feature map of the same spatial dimensions as $\mathbf{z}^{(l+1)}$. The use of computation blocks and lateral connections are ablated in Table 4. Figure 3 depicts a naive implementation that places both objectives at the top encoder level and PooDLLe, which uses the SDM to integrate the two objectives in a complementary fashion.

4 Experiments

We pretrain PooDLLe on raw videos from BDD100K [50] and Walking Tours (WT) [42] and evaluate them with semantic segmentation and object detection benchmarks. The BDD100K pretrained model is evaluated on the corresponding in-domain benchmarks as well as Cityscapes [14] and the Walking Tours model on ADE20K [1]. We also ablate our combination of loss functions and decoder components as well as the effects of crop area and input resolutions.

4.1 Experiment Setup

Pretraining datasets. 1) **BDD** [50] consists of 100,000 dashcam driving videos collected in various weather conditions and times of day from New York and the San Francisco Bay Area. Each video is 40 seconds long at 720p and 30 fps. We pretrain with the 70,000 videos in the official training split and evaluate on the semantic segmentation and object detection tasks proposed alongside the dataset. 2) **Walking Tours (WT)** [42] is a dataset of first-person egocentric videos collected from YouTube of a continuous walkaround through various cities of Europe, Asia, and a wildlife safari. There are 10 videos, ranging from 59 minutes to 2 hours 55 minutes, at 720p and 30 fps. Each video contains large numbers of unique objects per frame and natural transitions in lighting and location. For self-supervised pretraining, we use either the Venice video ($\text{WT}_{\text{Venice}}$) or all 10 videos (WT_{all}) following DoRA [42].

Technical details. We use ResNet-50 (R50) [23] as our feature encoder, with the dense projector and predictor networks following FlowE [49] and pooled counterparts following BYOL [20]. For SDM, we use two decoder stages, with each consisting of a $2\times$ upsample, a ResNet Bottleneck Block [23] for computation, and a 2-layer convolutional MLP for the lateral connection. When training on BDD, we sample two frames that are $0.5 \sim 1$ seconds apart ($\Delta t \in \{15\dots30\}$) from each video. We then take two large crops from the same image coordinates of area $[0.16, 0.45]$ of the original image and resize them to 512×1024 pixels before applying augmentations. For each training epoch on WT, we divide each video into 10-second clips and randomly sample two frames 0.5 seconds apart from each clip, and use crop area range $[0.65, 1.0]$. For non-spatial augmentations on both datasets, we apply color distortion and Gaussian blurring independently to each frame following BYOL [20]. For the dense objective, we also apply a random reversible affine transformations similar to FlowE [49]: random scaling of $0.9\text{--}1.1\times$ and rotation of $-10\text{--}10$. For the local objective, we sample $K = 6$ subcrop pairs and use a crop area of $[0.05, 0.3]$ of the initial dense crop for both BDD and WT, resized to 192×192 . When sampling subcrops, random spatial jitter is $\pm 10\%$ of the large crops’ height and width. We attempt experiments with ViT-S, but observe a collapse phenomenon (see Appendix G).

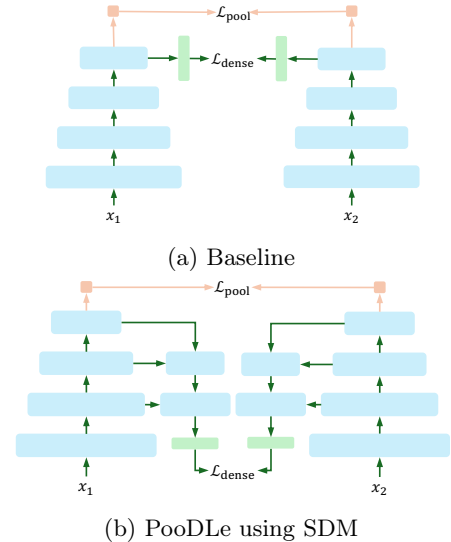


Figure 3: **a) Baseline:** both losses combined at final encoder layer; **b) PooDLLe:** SDM incorporates earlier feature maps to upsample for $\mathcal{L}_{\text{dense}}$.

Table 1: BDD semantic segmentation (SemSeg) and object detection (Det) readout evaluations. All settings are conducted with a frozen backbone. *Pretrained on BDD, initialized with supervised ImageNet weights.

Method	Arch	Ep.	Pretrain	BDD100K Sem. Seg.				BDD100K Obj. Det.		Cityscapes Sem. Seg			
				Linear		UperNet		Det C4	FPN	Linear		UperNet	
				mIoU	Acc	mIoU	Acc	mAP	mAP	mIoU	Acc	mIoU	Acc
Scratch	R50	-	-	9.7	55.0	26.1	81.2	0.0	7.7	9.8	58.0	30.7	84.1
DenseCL [45]	R50	800	BDD	21.3	82.6	46.9	91.4	0.9	23.4	25.1	84.8	57.2	93.0
FlowE [49]	R50	100	BDD	35.7	88.5	47.3	91.5	3.2	23.8	43.1	89.5	57.7	93.1
PixPro [48]	R50	100	BDD	21.8	80.0	37.3	88.0	0.7	18.4	25.5	81.0	44.3	89.5
DINO [7]	R50	100	BDD	13.1	64.7	25.6	80.3	0.3	11.9	14.9	69.4	29.2	81.4
DINO [7]	ViT-S	300	BDD	29.6	86.8	41.1	90.1	-	-	35.1	87.9	51.5	91.9
iBOT [54]	ViT-S	800	BDD	27.2	85.4	35.5	88.7	-	-	32.0	86.2	44.0	90.3
DoRA [42]	ViT-S	200	BDD	33.2	88.1	43.3	90.7	-	-	37.4	88.7	50.8	92.0
PooDLe	R50	100	BDD	39.2	89.2	49.9	91.8	4.9	25.2	47.2	90.2	60.7	93.5
Supervised	R50	600	IN1K	36.7	84.7	55.2	92.0	3.6	24.9	46.8	87.4	63.4	93.7
PooDLe	R50	100	BDD*	44.7	90.7	54.1	92.7	3.9	28.0	52.0	91.5	65.1	94.4

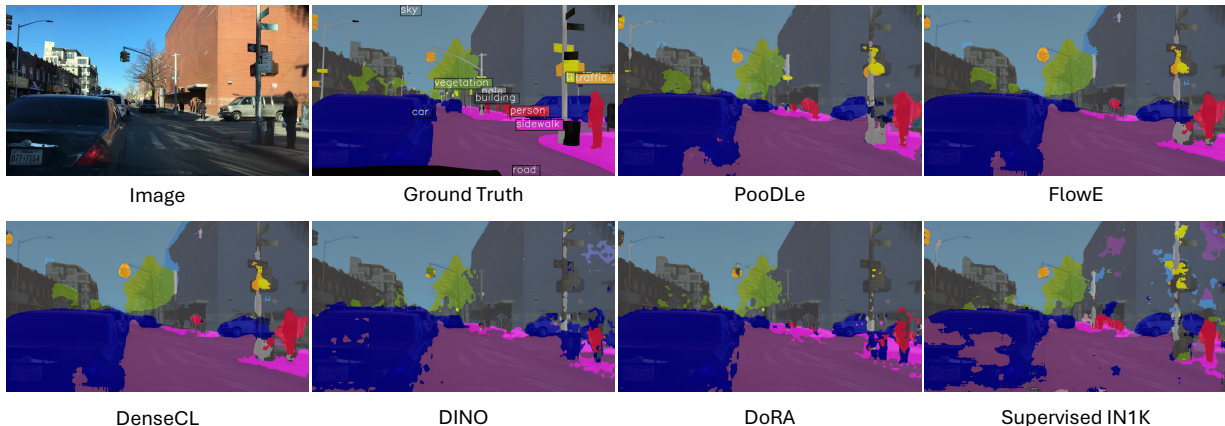


Figure 4: Visualization of BDD semantic segmentation linear readout. PooDLe is able to identify smaller objects and generate cleaner object boundaries.

Baselines. We use official implementations of DenseCL, PixPro, DINO, iBOT and DoRA, and our own implementation of FlowE for pretraining on BDD. We use `torchvision` for ImageNet supervised and weights released online for ImageNet-pretrained DINO. We obtain weights from the authors of DoRA for iBOT, DINO - ViT, and DoRA pretrained on WT and use official implementations of DINO - R50 and PixPro for pretraining on WT. For PixPro, we use its FPN decoder only in pretraining, which we find is best for performance. We use 512x1024 crops for training FlowE and DINO-R50; we are unable to train the other baselines with high-resolution crops due to prohibitive GPU memory requirements.

Evaluation. We adopt the evaluations described in FlowE [49] for BDD and Cityscapes. We use DeepLab v1 [10] as the ‘linear’ readout header and UperNet [47] as the heavier readout head for semantic segmentation and Faster R-CNN with ResNet-C4 and Faster R-CNN with FPN [24] as the standard and heavier readout headers for object detection. We do not include ViT object detection due to the lack of an existing reliable recipe. For semantic segmentation on ADE20K, we perform both linear readout following BDD and Upernet finetuning as described in iBOT [54]. We retain the SDM when evaluating PooDLe on semantic segmentation with linear readouts. We report mean intersection-over-union (mIoU), pixel-level accuracy (Acc), and mean average precision (mAP) as our evaluation metrics. Additional details on implementation and hyperparameters are provided in Appendix A.

Table 2: ADE20K semantic segmentation linear readout and finetuning evaluations. Linear readout is performed with a frozen backbone while in finetuning, backbone parameters are trainable. † DINO-ViT and iBOT results are taken from DoRA [42].

Method	Arch	Epoch	Pretrain	SemSeg Linear		Finetune	
				mIoU	Acc	mIoU	Acc
DINO [7]	R50	800	IN1K	15.7	61.5	43.0	80.5
DINO [7]†	ViT-S	100	IN1K	-	-	33.9	-
PixPro [48]	R50	100	WT _{Venice}	4.6	48.6	36.0	77.6
DINO [7]	R50	100	WT _{Venice}	6.9	48.2	35.7	77.4
DINO [7]	ViT-S	100	WT _{Venice}	7.8	57.7	29.2	74.7
iBOT [54]†	ViT-S	100	WT _{Venice}	-	-	33.9	-
DoRA [42]	ViT-S	100	WT _{Venice}	14.1	63.5	35.2	77.7
PooDLe	R50	20	WT _{Venice}	14.6	59.0	36.6	77.9
DoRA [42]	ViT-S	100	WT _{all}	13.9	64.4	38.3	79.3
PooDLe	R50	20	WT _{all}	16.5	63.9	41.0	79.6

4.2 Main Results

BDD100K-pretrained models. We evaluate the learned representations on semantic-segmentation and object-detection on the BDD in-distribution, labeled benchmark (Table 1). PooDLe achieves superior performance on all readout tasks compared to other models pretrained on BDD, outperforming the strongest baseline FlowE by 3.5% mIoU on linear and 2.6% mIoU on UperNet for semantic segmentation, and 1.7% mAP on C4 and 1.4% mAP on FPN for object detection. This indicates that PooDLe is able to learn better representations for dense prediction tasks. While we keep the decoder in linear readout, it is discarded during UperNet probing, showing that the representation improves substantially over all other BDD-trained models (49.9 mIoU compared to next-best 47.3). We demonstrate in Table 3 that our performance improvements are derived from better recognition of small classes. We also evaluate the downstream transfer of PooDLe representations by performing linear and UperNet readout on the Cityscapes benchmark with models trained on BDD. PooDLe readily outperforms all baselines. We provide visualizations of predicted segmentation masks in Figure 4 and additional evaluation visualizations in Figure 12 and Figure 13.

PooDLe outperforms ImageNet supervised pretraining as well, despite the latter’s advantage in learning small and rare classes present in BDD100K (spatial imbalance shown in Figure 1) due to ImageNet being a class-balanced dataset with iconic views of objects. In addition, we may pretrain PooDLe on BDD100K with weights initialized from the ImageNet supervised checkpoint to further improve performance, notably boosting mIoU by 8% and Acc by 6% on linear semantic segmentation. We provide additional comparisons to ImageNet-pretrained baselines in Appendix E, where PooDLe remains competitive despite being pretrained in the challenging naturalistic video setting.

WT-pretrained models. We also train PooDLe on WT_{Venice} as well as the entire dataset, WT_{all}. Table 2 shows linear readout and finetuning experiments on ADE20K [53] semantic segmentation following Venkataraman et al. [42]. Notably, when pretrained on WT_{all}, PooDLe surpasses DoRA by 2.6% mIoU on linear readout and 2.7% mIoU on UperNet finetuning over DoRA. PooDLe also shows some improvement trained on WT_{Venice}-pretraining setting, with a gain of 0.5% mIoU on linear readout over DoRA and 0.6% mIoU on UperNet finetuning over PixPro. This shows that PooDLe also learns strong representations from naturalistic video captured in the open world. We show visualizations of predicted segmentation masks for ADE20K evaluations in Figure 14.

Class-based performance and IN1K initialization. Naturalistic videos have severe class and size imbalance (Figure 1c; e.g., for semantic segmentation, the "road" occupies 21% of pixels and appears in 96% of images while "bicycle" only occupies 0.05% in 6% of images). Capturing information on severely underrepresented classes is very challenging. While it is unfeasible to balance our training data, we demonstrated the composability of PooDLe with iconic pretraining by initializing with supervised ImageNet weights (Table 1). This variant improves upon the semantic class understanding of IN1K-pretraining while also significantly improving on spatial boundaries (accuracy), which we hypothesize is due to our dense loss $\mathcal{L}_{\text{dense}}$.

Table 3: Breakdowns of mIoU over different class groupings. Linear readout mIoU is computed over various groupings of the 19 classes in BDD semantic segmentation. *Pretrained on BDD, initialized with supervised ImageNet weights.

Method	Pretrain	All	Small	Large	Rare	Common
DINO	BDD	29.6	8.4	42.0	1.0	42.8
DenseCL	BDD	21.7	1.6	33.4	0.0	31.7
DoRA	BDD	33.2	11.9	45.6	2.8	47.3
FlowE	BDD	35.7	12.2	49.3	10.7	47.2
PooDLe	BDD	39.2	18.3	51.4	12.0	51.8
Supervised	IN1K	36.7	27.2	42.2	16.1	46.2
PooDLe	BDD*	44.7	25.2	56.1	17.9	57.1

Table 4: Ablation studies on PooDLe components, reporting mIoU on BDD100K semantic segmentation linear readout. Rows without top-down follow FlowE [49], replacing pooling with dilated convolutions to maintain spatial extent. †Flow model trained without supervised labels.

Variant	Dense	Pool	Top-Down	Lateral	Flow	All	Small	Large	Rare	Common
1 FlowE	✓				RAFT	28.8	8.7	40.5	1.8	29.2
2	✓	✓			RAFT	28.9	7.2	41.6	2.2	28.7
3	✓	✓	✓		RAFT	30.3	6.8	44.0	4.3	30.2
4	✓	✓		✓	RAFT	30.3	10.9	41.7	2.4	31.1
5	✓		✓	✓	RAFT	31.8	12.8	42.8	8.3	31.7
6 PooDLe†	✓	✓	✓	✓	UFlow	33.7	14.1	45.1	8.9	33.8
7 PooDLe	✓	✓	✓	✓	RAFT	34.2	15.0	45.5	9.0	34.5

In particular, training PooDLe on BDD improves performance on linear readout by 8% mIoU and 6% Acc over the supervised IN1K weights used for initialization.

To further evidence this phenomenon, we designate BDD classes as "small" if they on average occupy < 1% of pixels and "large" as those that occupy > 1%. We also independently define "rare" as classes that appear in < 20% of images and "common" as those that appear > 20%. Table 3 shows linear readout mIoU with different class groupings to further illustrate the class and spatial imbalance effect. Full class-level statistics and designations are in Appendix F. We observe that FlowE performs well on large and common classes due to its dense loss, but struggles on small or rare classes. Meanwhile, the supervised ImageNet model effectively learns about smaller classes via its balanced pretraining data as evidenced by its performance on semantic segmentation. PooDLe, with its unified objectives, and spatial decoder module shows significant improvement over other BDD-trained models in all class designations and particularly on small and rare classes. We also train a PooDLe on top of supervised ImageNet weights. It drastically improves on large classes, from 42.2% to 56.1%, due to the dense objective, while remaining competitive with supervised ImageNet on small classes.

4.3 Ablation studies

Table 4 shows our ablation experiments, testing each of our contributions beginning from FlowE. Models trained without the decoder use dilated convolutions in place of pooling operations, as in FlowE [49]. How the dense and pooled objectives are composed with and without the decoder is shown in Figure 3. For this table, models are trained for 40 epochs on BDD and use a reduced 256×512 resolution and $[0.04, 0.11]$ area for the initial crops; we evaluate on BDD semantic segmentation using linear readout.

We observe that adding \mathcal{L}_{pool} alone has little benefit (row 2) and including either the decoder as a spatial upsampler (row 3) or only the UNet-style lateral connections (row 4) also does not yield much benefit. Row 5 achieves +3% mIoU, showing that the top-down decoder is only effective when combined with the lateral connections for the full SDM, suggesting that preserving high-resolution information as well as including some capacity for feature processing are both important. However, when re-adding the pooled loss in addition to the decoder *with* lateral connections (row 7), we see a substantial 5.4% mIoU improvement. While the

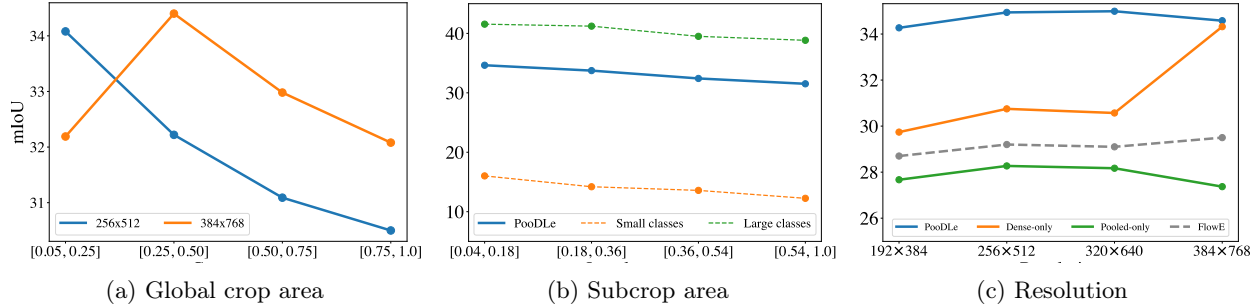


Figure 5: Experiments varying image cropping parameters for global and subcrops. (a) vary global crop area (b) varying subcrop area with effect on large and small class groups (c) jointly varying global crop area and input resolution to keep constant pixel density.



Figure 6: Varying initial crop area as a percent of the full frame. As crop area decreases, the views transition from global views of a dense scene to pseudo-iconic views, sometimes depicting singular subjects.

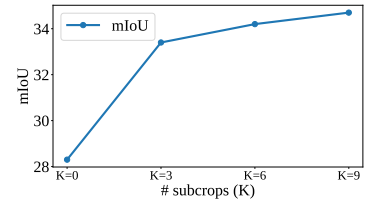


Figure 7: mIoU when varying number of subcrops K .

dense objective benefits from the full SDM, it has an even greater synergistic effect with the pooled loss. This may be because the pooled objective with subcrops can effectively learn about small objects while the full decoder helps propagate the semantic representations through to the dense loss.

We also demonstrate that PooDLe is able to perform well even with self-supervised flow. We train our own unsupervised UFlow [30] model on KITTI [18] and finetune it on BDD resulting in only a 0.5% mIoU loss compared to pretraining with RAFT. See Appendix H and A for visualizations and details.

4.4 Spatial and temporal cropping in self-supervised video learning

In this section, we study the effect of image cropping parameters used during data augmentation. As there is no longer a 1:1 image-to-concept relationship like in iconic data, how much of a scene is visible and assigned to each representation can greatly affect learning. Specifically, we perform 5 experiments varying: (1) global crop area, (2) subcrop area, and (3) global crop area and resolution to preserve pixel density (4) number of subcrops (5) temporal stride Δt . Crop area refers to the fraction of an image taken by the crop, and pixel density is the ratio of source frame pixels to model input frame pixels. Figure 6 visually depicts how crops transition from global to pseudo-iconic with decreasing crop area. Training recipe follows the ablations in section 4.3 and should be compared to row 7 in Table 4.

Varying global crop area when training PooDLes. We train 4 PooDLes on non-overlapping crop ranges $(a_{\min}, a_{\max}) = (0.05, 0.25), (0.25, 0.50), (0.50, 0.75), (0.75, 1.0)$, and 2 different resolutions 256×512 and 384×768 . Results are shown in Figure 5a. We find that directly increasing crop area, thereby increasing the content seen by each vector in $\mathcal{L}_{\text{dense}}$, does not directly improve performance. Rather, there is a sweet spot for each resolution, $[0.05, 0.25]$ for 256×512 and $[0.25, 0.5]$ for 384×768 with the larger resolution performing slightly better (34.0% v. 34.4%). While larger global crop areas improve PooDLe representations, they must be paired with a larger input resolution, otherwise performance degrades. We believe this is due to loss of information from downsampling.

Varying subcrop area. Next, we study how subcrop area affects our learned representations. Again, we train 4 PooDLes on subcrop ranges, using a fixed global crop range $[0.125, 0.25]$ at resolution 256×512 . Results are shown in Figure 5b. We show the mIoU for all classes, as well as the large and small class



Figure 8: Overlaid frames with varying Δt .

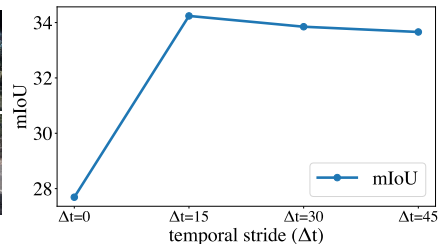


Figure 9: mIoU when varying Δt .

subgroupings. We observe that larger subcrop areas result in poorer performance, which we hypothesize is due to how larger subcrops are more likely to contain multiple subjects, producing false invariances. In addition, when crops are too large, subcrops may not serve well as pseudo-iconic views.

Varying input resolution with fixed pixel density. With the above observation, we train another set of models while controlling the pixel density. The frame crop area is set to $[0.125, 0.25]$ and the base crop size, 256×512 making the average pixel density $\rho_{\text{pixel}} = 1.32$. Maintaining this pixel density, we extrapolate 3 additional scales with input resolution $H \times W = (192 \times 384), (320 \times 640), (384 \times 768)$ and crop range $(0.07, 0.14), (0.195, 0.39), (0.281, 0.563)$. We pretrain a PooDLe as well as dense-only, pooled-only, and FlowE models for each scale on BDD100K and evaluate using linear readout. As subcrops are taken from global crops, we adjust the local crop area following Figure 5b for 320×640 and 384×768 to $(0.032, 0.192)$ and $(0.022, 0.133)$.

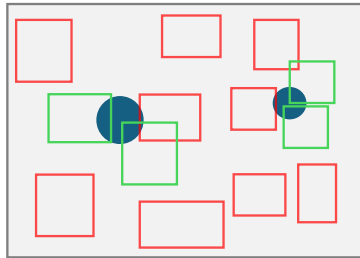
The results in Figure 5c confirm our hypotheses. PooDLe trained with both objectives is more robust to different input scopes given a fixed pixel density whereas a dense-only model requires high resolution, and pooled-only and FlowE are less competitive on all resolutions.

Varying number of subcrops We also study how varying the number of subcrops affects performance. We train 4 PooDLes using $K = 0, 3, 6, 9$ subcrops on BDD100K and evaluate using linear readout, with results shown in Figure 7. Using 3 subcrops gives an initial large performance jump and using additional subcrops provides more modest gains. We decide to use $K = 6$ as our default option to balance between performance and computational efficiency.

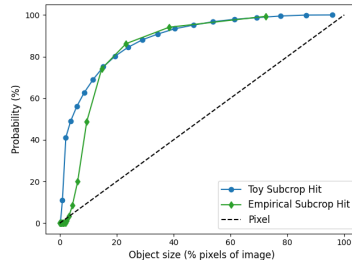
Effect of temporal stride during frame sampling. To study the effect of varying Δt , we train PooDLe with values $\Delta t = 0, 15, 30, 45$ on BDD100K and once again evaluate using linear readout (Figure 9). Performance degrades when temporal stride is either too small or too large. When it is small, there is limited variance in object appearance, making the training objective too easy. On the other hand, as temporal stride grows, correspondence between frames decreases and optical flow may become unreliable. Note that for $\Delta t = 0$, we jitter the initial large crop by up to 10% of the image size. We also visualize frame sequences from 3 different videos, Figure 8 showing the high variability of motion in BDD100K.

4.5 Subcrops as pseudo-iconic training images

We find that the addition of a pooled loss on pseudo-iconic subcrops improves PooDLe representations, particularly on smaller objects. To better understand this effect, we analyze how subcrops may increase the prevalence of small objects when they are assumed to be pseudo-iconic. First, we simulate a circle as our foreground object and compute the probability that a subcrop “hits” the object as a pseudo-iconic view, as illustrated in Figure 10a. A subcrop counts as a hit if at least 5% of the subcrop is occupied by the object. We argue that this is a reasonable assumption because background classes typically contain little visual variation and thus, have a relatively modest effect on the learned pooled representations. We also empirically simulate subcrops on the BDD100K semantic segmentation training dataset, and compute subcrop hit and pixel probabilities for foreground objects of varying size. As shown in Figure 10b, the relative difference between the subcrop probability and pixel probability is greater for smaller objects. This illustrates how subcrops can boost prevalence of small foreground objects in the pooled objective in comparison to the pixel-level dense SSL objective. Appendix C contains additional details about our setup and analyses.



(a) Toy simulation to compute probability of subcrop acting as a pseudo-iconic view, i.e. hit, of circular object. Subcrop hits are green and non-hits are red.



(b) Subcrop and pixel probabilities for foreground objects of varying size from toy and empirical simulation.

Figure 10: Analysis of subcrops as pseudo-iconic views.

5 Conclusion

Self-supervised learning on naturalistic videos present many unsolved challenges, especially due to the presence of high-resolution multi-object crowded scenes with severe spatial region imbalance. Iconic methods rely on single-subject images and dense methods struggle with scale-imbalance of objects. We propose PooDLe that combines pooled region-invariance learning and dense flow-equivariance learning objectives in a unified framework. PooDLe achieves state-of-the-art performance on downstream semantic evaluations compared to prior methods pretrained on the same video datasets, particularly on recognizing small objects. Our study on the effects of crop area, resolution density, and temporal stride also offers key insights on the design choices for video self-supervised learning.

Limitations and future work. Our work has several limitations and areas for future work. First, PooDLe relies on an external flow prediction network. Although we demonstrate that an unsupervised flow predictor also works well, it would be more elegant to incorporate motion prediction in a joint framework like in MC-JEPA [5]. Additionally, while PooDLe achieves state-of-the-art performance, we find that it does not currently work well with ViTs and this limitation warrants further investigations. In the future, we would also like to explore ways to zoom-in and attend to interesting regions and regions that contain rare objects rather than relying on random subcrops, e.g., using priors such as motion [13, 28] to identify foreground objects.

Acknowledgment

We would like to thank Adrien Bardes and Jean Ponce for helpful discussion, and the Microsoft Accelerating Foundation Models Research program for providing cloud compute credits for our experiments. The project was also supported by the NYU High Performance Computing resources, services, and staff expertise.

References

- [1] Pulkit Agrawal, Joao Carreira, and Jitendra Malik. Learning to see by moving. In *Proceedings of the IEEE International Conference on Computer Vision*, 2015.
- [2] Mahmoud Assran, Quentin Duval, Ishan Misra, Piotr Bojanowski, Pascal Vincent, Michael Rabbat, Yann LeCun, and Nicolas Ballas. Self-supervised learning from images with a joint-embedding predictive architecture. In *Proceedings of the IEEE/CVF Conference on Computer Vision and Pattern Recognition*, 2023.
- [3] Adrien Bardes, Jean Ponce, and Yann LeCun. Vicreg: Variance-invariance-covariance regularization for self-supervised learning. In *International Conference on Learning Representations*, 2021.
- [4] Adrien Bardes, Quentin Garrido, Jean Ponce, Xinlei Chen, Michael Rabbat, Yann LeCun, Mido Assran, and Nicolas Ballas. V-jepa: Latent video prediction for visual representation learning. *arXiv preprint arXiv:2404.08471*, 2023.
- [5] Adrien Bardes, Jean Ponce, and Yann LeCun. Mc-jepa: A joint-embedding predictive architecture for self-supervised learning of motion and content features. *arXiv preprint arXiv:2307.12698*, 2023.
- [6] Mathilde Caron, Ishan Misra, Julien Mairal, Priya Goyal, Piotr Bojanowski, and Armand Joulin. Unsupervised learning of visual features by contrasting cluster assignments. In *Advances in Neural Information Processing Systems*, 2020.
- [7] Mathilde Caron, Hugo Touvron, Ishan Misra, Hervé Jégou, Julien Mairal, and Armand Joulin. Emerging properties in self-supervised vision transformers. In *IEEE/CVF International Conference on Computer Vision*, 2021.
- [8] Kai Chen, Lanqing Hong, Hang Xu, Zhenguo Li, and Dit-Yan Yeung. Multisiam: Self-supervised multi-instance siamese representation learning for autonomous driving. In *Proceedings of the IEEE/CVF International Conference on Computer Vision*, 2021.
- [9] Liang-Chieh Chen, George Papandreou, Florian Schroff, and Hartwig Adam. Rethinking atrous convolution for semantic image segmentation. *arXiv preprint arXiv:1706.05587*, 2017.
- [10] Liang-Chieh Chen, George Papandreou, Iasonas Kokkinos, Kevin Murphy, and Alan L. Yuille. Deeplab: Semantic image segmentation with deep convolutional nets, atrous convolution, and fully connected crfs. *IEEE Transactions on Pattern Analysis and Machine Intelligence*, 2018.
- [11] Ting Chen, Simon Kornblith, Mohammad Norouzi, and Geoffrey Hinton. A simple framework for contrastive learning of visual representations. In *International Conference on Machine Learning*, 2020.
- [12] Xinlei Chen and Kaiming He. Exploring simple siamese representation learning. In *Proceedings of the IEEE/CVF Conference on Computer Vision and Pattern Recognition*, 2021.
- [13] Subhabrata Choudhury, Laurynas Karazija, Iro Laina, Andrea Vedaldi, and Christian Rupprecht. Guess What Moves: Unsupervised Video and Image Segmentation by Anticipating Motion. In *British Machine Vision Conference*, 2022.
- [14] Marius Cordts, Mohamed Omran, Sebastian Ramos, Timo Rehfeld, Markus Enzweiler, Rodrigo Benenson, Uwe Franke, Stefan Roth, and Bernt Schiele. The cityscapes dataset for semantic urban scene understanding. In *Proceedings of the IEEE/CVF Conference on Computer Vision and Pattern Recognition*, 2016.
- [15] Jia Deng, Wei Dong, Richard Socher, Li-Jia Li, Kai Li, and Li Fei-Fei. Imagenet: A large-scale hierarchical image database. In *Proceedings of the IEEE/CVF Conference on Computer Vision and Pattern Recognition*, 2009.

- [16] Alexey Dosovitskiy, Lucas Beyer, Alexander Kolesnikov, Dirk Weissenborn, Xiaohua Zhai, Thomas Unterthiner, Mostafa Dehghani, Matthias Minderer, Georg Heigold, Sylvain Gelly, Jakob Uszkoreit, and Neil Houlsby. An image is worth 16x16 words: Transformers for image recognition at scale. In *International Conference on Learning Representations*, 2021.
- [17] Christoph Feichtenhofer, Yanghao Li, Kaiming He, et al. Masked autoencoders as spatiotemporal learners. In *Advances in Neural Information Processing Systems*, 2022.
- [18] Andreas Geiger, Philip Lenz, Christoph Stiller, and Raquel Urtasun. Vision meets robotics: The kitti dataset. *International Journal of Robotics Research*, 2013.
- [19] Daniel Gordon, Kiana Ehsani, Dieter Fox, and Ali Farhadi. Watching the world go by: Representation learning from unlabeled videos. *arXiv preprint arXiv:2003.07990*, 2020.
- [20] Jean-Bastien Grill, Florian Strub, Florent Altché, Corentin Tallec, Pierre H. Richemond, Elena Buchatskaya, Carl Doersch, Bernardo Ávila Pires, Zhaohan Daniel Guo, Mohammad Gheshlaghi Azar, Bilal Piot, Koray Kavukcuoglu, Rémi Munos, and Michal Valko. Bootstrap your own latent: A new approach to self-supervised learning. In *Advances in Neural Information Processing Systems*, 2020.
- [21] Qiushan Guo, Yizhou Yu, Yi Jiang, Jiannan Wu, Zehuan Yuan, and Ping Luo. Multi-level contrastive learning for dense prediction task. *arXiv preprint arXiv:2304.02010*, 2023.
- [22] Agrim Gupta, Jiajun Wu, Jia Deng, and Fei-Fei Li. Siamese masked autoencoders. In *Advances in Neural Information Processing Systems*, pages 40676–40693. Curran Associates, Inc., 2023.
- [23] Kaiming He, Xiangyu Zhang, Shaoqing Ren, and Jian Sun. Deep residual learning for image recognition. In *Proceedings of the IEEE/CVF Conference on Computer Vision and Pattern Recognition*, 2016.
- [24] Kaiming He, Xiangyu Zhang, Shaoqing Ren, and Jian Sun. Deep residual learning for image recognition. In *Proceedings of the IEEE/CVF Conference on Computer Vision and Pattern Recognition*, 2016.
- [25] Kaiming He, Haoqi Fan, Yuxin Wu, Saining Xie, and Ross Girshick. Momentum contrast for unsupervised visual representation learning. In *Proceedings of the IEEE/CVF Conference on Computer Vision and Pattern Recognition*, 2020.
- [26] Kaiming He, Xinlei Chen, Saining Xie, Yanghao Li, Piotr Dollár, and Ross Girshick. Masked autoencoders are scalable vision learners. In *Proceedings of the IEEE/CVF Conference on Computer Vision and Pattern Recognition*, 2022.
- [27] Olivier J Hénaff, Skanda Koppula, Jean-Baptiste Alayrac, Aaron Van den Oord, Oriol Vinyals, and Joao Carreira. Efficient visual pretraining with contrastive detection. In *Proceedings of the IEEE/CVF International Conference on Computer Vision*, 2021.
- [28] Richard EL Higgins and David F Fouhey. Moves: Manipulated objects in video enable segmentation. In *Proceedings of the IEEE/CVF Conference on Computer Vision and Pattern Recognition*, 2023.
- [29] Allan Jabri, Andrew Owens, and Alexei Efros. Space-time correspondence as a contrastive random walk. *Advances in Neural Information Processing Systems*, 2020.
- [30] Rico Jonschkowski, Austin Stone, Jonathan Barron, Ariel Gordon, Kurt Konolige, and Anelia Angelova. What matters in unsupervised optical flow. In *European Conference on Computer Vision*, 2020.
- [31] Tsung-Yi Lin, Piotr Dollár, Ross Girshick, Kaiming He, Bharath Hariharan, and Serge Belongie. Feature pyramid networks for object detection. In *Proceedings of the IEEE/CVF Conference on Computer Vision and Pattern Recognition*, 2017.
- [32] Pengpeng Liu, Irwin King, Michael R Lyu, and Jia Xu. DdfLOW: Learning optical flow with unlabeled data distillation. In *Proceedings of the AAAI Conference on Artificial Intelligence*, 2019.

- [33] Aaron van den Oord, Yazhe Li, and Oriol Vinyals. Representation learning with contrastive predictive coding. *arXiv preprint arXiv:1807.03748*, 2018.
- [34] Maxime Oquab, Timothée Darcet, Théo Moutakanni, Huy Vo, Marc Szafraniec, Vasil Khalidov, Pierre Fernandez, Daniel Haziza, Francisco Massa, Alaaeldin El-Nouby, et al. Dinov2: Learning robust visual features without supervision. *Transactions on Machine Learning Research*, 2023.
- [35] Nikhil Parthasarathy, SM Eslami, Joao Carreira, and Olivier Henaff. Self-supervised video pretraining yields robust and more human-aligned visual representations. *Advances in Neural Information Processing Systems*, 2023.
- [36] Xiangyu Peng, Kai Wang, Zheng Zhu, Mang Wang, and Yang You. Crafting better contrastive views for siamese representation learning. In *Proceedings of the IEEE/CVF Conference on Computer Vision and Pattern Recognition*, 2022.
- [37] Alec Radford, Jong Wook Kim, Chris Hallacy, Aditya Ramesh, Gabriel Goh, Sandhini Agarwal, Girish Sastry, Amanda Askell, Pamela Mishkin, Jack Clark, et al. Learning transferable visual models from natural language supervision. In *International Conference on Machine Learning*, 2021.
- [38] Olaf Ronneberger, Philipp Fischer, and Thomas Brox. U-net: Convolutional networks for biomedical image segmentation. In *Medical Image Computing and Computer-Assisted Intervention International Conference*, 2015.
- [39] Ramprasaath R. Selvaraju, Karan Desai, Justin Johnson, and Nikhil Naik. Casting your model: Learning to localize improves self-supervised representations. In *Proceedings of the IEEE/CVF Conference on Computer Vision and Pattern Recognition*, 2021.
- [40] Zachary Teed and Jia Deng. Raft: Recurrent all-pairs field transforms for optical flow. In *European Conference on Computer Vision*, 2020.
- [41] Zhan Tong, Yibing Song, Jue Wang, and Limin Wang. Videomae: Masked autoencoders are data-efficient learners for self-supervised video pre-training. In *Advances in Neural Information Processing Systems*, 2022.
- [42] Shashanka Venkataramanan, Mamshad Nayeem Rizve, João Carreira, Yuki M Asano, and Yannis Avrithis. Is imagenet worth 1 video? learning strong image encoders from 1 long unlabelled video. In *International Conference on Learning Representations*, 2024.
- [43] Pascal Vincent, Hugo Larochelle, Isabelle Lajoie, Yoshua Bengio, and Pierre-Antoine Manzagol. Stacked denoising autoencoders: Learning useful representations in a deep network with a local denoising criterion. *Journal of Machine Learning Research*, 2010.
- [44] Wenguan Wang, Tianfei Zhou, Fisher Yu, Jifeng Dai, Ender Konukoglu, and Luc Van Gool. Exploring cross-image pixel contrast for semantic segmentation. In *Proceedings of the IEEE/CVF International Conference on Computer Vision*, 2021.
- [45] Xinlong Wang, Rufeng Zhang, Chunhua Shen, Tao Kong, and Lei Li. Dense contrastive learning for self-supervised visual pre-training. In *Proceedings of the IEEE/CVF Conference on Computer Vision and Pattern Recognition*, 2021.
- [46] Philippe Weinzaepfel, Vincent Leroy, Thomas Lucas, Romain Brégier, Yohann Cabon, Vaibhav Arora, Leonid Antsfeld, Boris Chidlovskii, Gabriela Csurka, and Jérôme Revaud. Croco: Self-supervised pre-training for 3d vision tasks by cross-view completion. *Advances in Neural Information Processing Systems*, 2022.
- [47] Tete Xiao, Yingcheng Liu, Bolei Zhou, Yuning Jiang, and Jian Sun. Unified perceptual parsing for scene understanding. In *Proceedings of the European Conference on Computer Vision*, 2018.

- [48] Zhenda Xie, Yutong Lin, Zheng Zhang, Yue Cao, Stephen Lin, and Han Hu. Propagate yourself: Exploring pixel-level consistency for unsupervised visual representation learning. In *Proceedings of the IEEE/CVF Conference on Computer Vision and Pattern Recognition*, 2021.
- [49] Yuwen Xiong, Mengye Ren, Wenyuan Zeng, and Raquel Urtasun. Self-supervised representation learning from flow equivariance. In *Proceedings of the IEEE/CVF International Conference on Computer Vision*, 2021.
- [50] Fisher Yu, Haofeng Chen, Xin Wang, Wenqi Xian, Yingying Chen, Fangchen Liu, Vashisht Madhavan, and Trevor Darrell. Bdd100k: A diverse driving dataset for heterogeneous multitask learning. In *Proceedings of the IEEE/CVF Conference on Computer Vision and Pattern Recognition*, 2020.
- [51] Jure Zbontar, Li Jing, Ishan Misra, Yann LeCun, and Stéphane Deny. Barlow twins: Self-supervised learning via redundancy reduction. In *International Conference on Machine Learning*, 2021.
- [52] Shaofeng Zhang, Feng Zhu, Rui Zhao, and Junchi Yan. Patch-level contrasting without patch correspondence for accurate and dense contrastive representation learning. In *International Conference on Learning Representations*, 2023.
- [53] Bolei Zhou, Hang Zhao, Xavier Puig, Sanja Fidler, Adela Barriuso, and Antonio Torralba. Scene parsing through ade20k dataset. In *Proceedings of the IEEE/CVF Conference on Computer Vision and Pattern Recognition*, 2017.
- [54] Jinghao Zhou, Chen Wei, Huiyu Wang, Wei Shen, Cihang Xie, Alan Yuille, and Tao Kong. ibot: Image bert pre-training with online tokenizer. In *International Conference on Learning Representations*, 2021.
- [55] Adrian Ziegler and Yuki M Asano. Self-supervised learning of object parts for semantic segmentation. In *Proceedings of the IEEE/CVF Conference on Computer Vision and Pattern Recognition*, 2022.

Appendix

A Implementation details

Backbone. As discussed in the pretraining details, we use a Resnet-50 [23] as our backbone architecture. The projector model is a non-linear, 2-layer MLP (linear for pooled, 1×1 convolutions for dense) that has a 4096 hidden dimension and projects down to 256 dimensions. The predictor is the same network with $256 - 4096 - 256$ channels. We follow BYOL [20] with a momentum starting at 0.996 and increases to 1 throughout training.

Decoder details. The decoder uses a single Bottleneck block from the ResNet architecture with a $8 \times$ downsampling ratio in the number of channels. Upsampling in the decoder is $2 \times$ and the lateral connection is a single linear convolutional layer that up-projects the input latent to match the decoder channels ($1024 \rightarrow 2048$ in the first decoder block and $512 \rightarrow 2048$ for the second block). As mentioned, 2 decoder blocks are used to achieve a total of $4 \times$ upsampling.

Supervised and self-supervised flow prediction. Flow is predicted using a supervised off-the-shelf RAFT model or an unsupervised UFlow [30] model that we train ourselves. For unsupervised training, we exactly follow UFlow and train on the KITTI [18] dataset before finetuning on BDD100k [50] for 100000 steps on daytime-only videos. The training and inference resolutions were set to 256×512 to better match the inference setting. KITTI used adjacent frames (10Hz video) while BDD frames were sampled with temporal stride of 10 (30Hz video).

Local cropping details. $K = 6$ paired local crops are sampled using the methods described. Cropping is performed using RandomResizedCrop with an output resolution of 192×192 . Jitter is 10% of the input image size and standard aspect ratio range of $[3/4, 4/3]$ is used.

Loss details. We sum our 2 loss functions directly and give them equal weight. The loss computation and warping function were applied to representations after reversing the affine transform and resizing to the input image resolution, this is to take full advantage of high resolution flow like in FlowE [49]. We also use flow-based occlusion to prevent misaligning occluded regions without correspondence. We use the same occlusion formulation as DDFlow [32] and parameters $\alpha_1 = 0.1, \alpha_2 = 0.5$. We also mask out regions that are not visible after affine transformations for $\mathcal{L}_{\text{dense}}$.

Our loss is symmetrical: we reverse the x_t and $x_{t+\Delta}$ so that both are encoded by the online weights and used for optimization at each training step.

Optimization details. AdamW is used as the optimizer and a weight decay value of 0.01. A learning rate of $5e - 4$ is used with batch size of 32 GPUs and 4 image pairs per GPU for a batch size total of 128. Cosine learning rate decay is used with a schedule for 300 epochs, despite early termination due to compute limitations. LR warmup is used for 2 training epochs. Full `float32` precision is used during training.

Evaluation settings. For all BDD and Cityscapes semantic segmentation and object detection readout tasks, we follow the setup described in FlowE [49] for ResNet-based methods. For ViT-based methods, we adopt those settings, but use AdamW for the optimizer with learning rate of $3e - 5$ and weight decay of 0.05, and a crop size of 512×512 rather than the normal 512×1024 to accommodate the square aspect ratio used in ViT-pretraining, following the semantic segmentation linear readout setup described in iBOT [54]. In addition, ViT-based methods require sliding window inference in order to achieve performance that is competitive with convolution-based methods.

For ADE20K linear readout, we simply use the respective BDD linear readout settings for ResNet and ViT methods. For ADE20K UperNet finetuning, we follow the procedure described in iBOT [54].

Ablation data sampling. For all ablation experiments, we employ repeated sampling like in MAE-st [17] which samples R frames each time a video is encountered for faster data loading. Therefore, each pass through every video in the dataset counts as R epochs.

B Compute resources

The full model is trained on 16 A100s and takes about 30h for 100 epochs on BDD100K or 18min per epoch. Walking Tours takes longer at 40min per epoch, as the number of training samples per epoch is larger.

Ablation-sized experiments were run 2 or 4 H100/A100 GPUs for a total of 40 epochs taking 20-40h depending on the configuration.

C Subcrop analysis

For the toy simulation of subcrops, we place a foreground object as a centered circle of varying size within a 256×512 frame. We then simulate all possible subcrops of area $A \in [0.02, 0.04, 0.06, 0.08]$. For each subcrop area, we compute subcrop hits, i.e. whether at least 5% of the subcrop contains the object, using numerical grid-based integration. We compute the subcrop hit probability, or subcrop hits over valid subcrops, averaged across subcrop areas, as well as the pixel probability, or object pixels over total image pixels.

We also emulate our training procedure for our empirical simulation of subcrops. For each of the 7,000 images in the BDD100K semantic segmentation training dataset, we sample two global crops with area sampled from $U[0.16, 0.45]$ and for each global crop, 4096 subcrops with area sampled from $U[0.02, 0.03]$. We compute subcrop probability and pixel probability independently for the pixels of each foreground class: pole, traffic light, traffic sign, person, rider, car, truck, bus, train, motorcycle, bicycle. We then group the results into 10% quantile bins by object size (i.e. pixel proportions) and average the subcrop and pixel probabilities. We utilize a slightly different subcrop area range in the empirical simulation because our two-step global crop and subcrop procedure results in a logarithmic-like distribution.

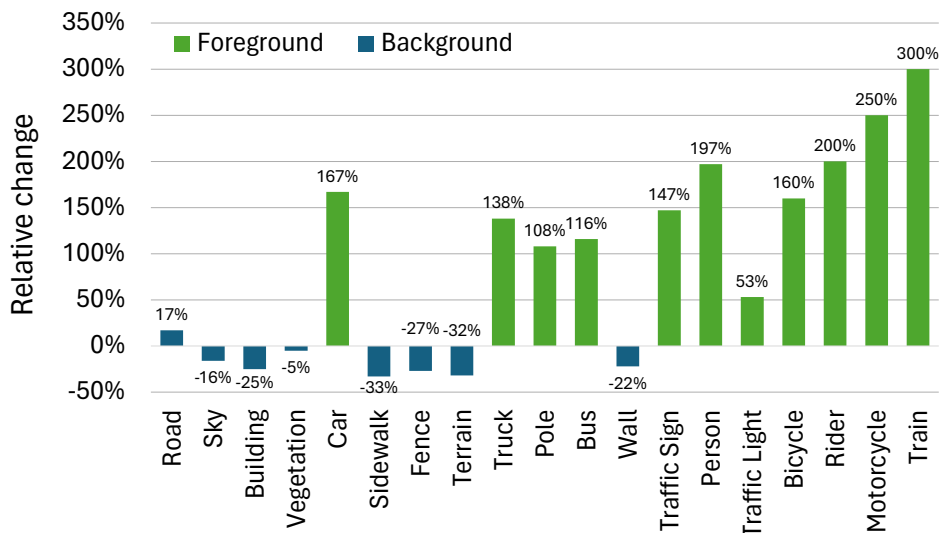


Figure 11: Relative change in local crop region class assignments relative to per-pixel class distribution.

We hypothesize that PooDLe’s improvement on spatially underrepresented classes, as shown in Table 7, is due to this subcrop effect. To quantify this effect on real data, we perform a similar exercise as above on the BDD100K semantic segmentation training set. We sample subcrops following our method and assign a class label to each subcrop. If over 10% of the subcrop is a foreground class (*not* road, sky, building, vegetation, sidewalk, fence, terrain), then we label the subcrop as the majority foreground class. Otherwise, the majority background class label is assigned. In Figure 11, we show the relative change in class distribution when using this subcrop class assignment. Foreground classes (green) increase in occurrence while background classes (blue) decrease in frequency, besides road.

D Additional visualizations

We provide additional visualizations of results on our evaluated benchmarks: BDD100K [50] semantic segmentation (Figure 12), object detection (Figure 13) and ADE20K semantic segmentation (Figure 14). Once again, we note that PooDL produces segmentation maps with clearer boundaries while also effectively capturing small objects.

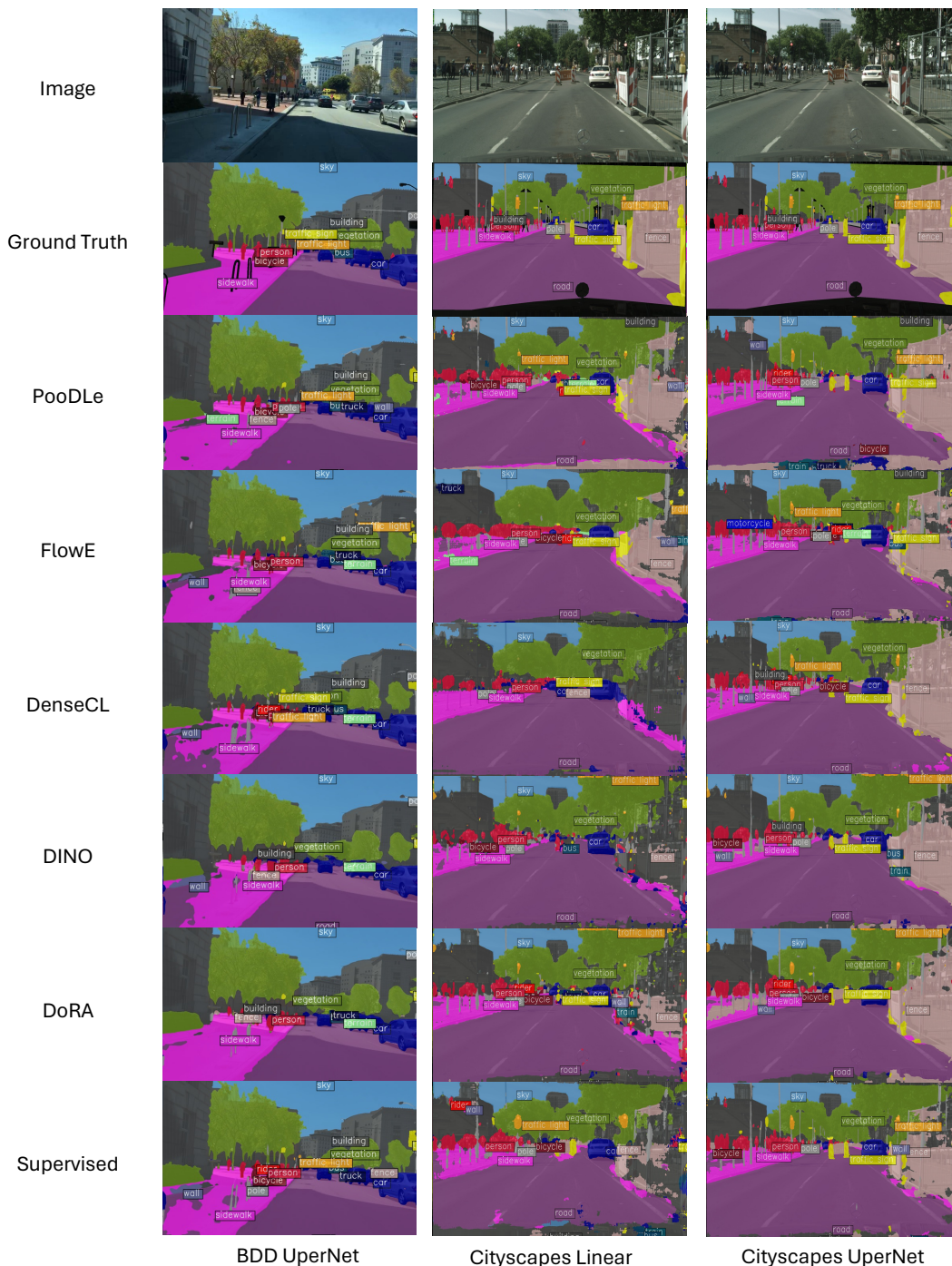


Figure 12: Visualizations of semantic segmentation masks for BDD linear readout, Cityscapes linear readout, and Cityscapes UperNet readout.

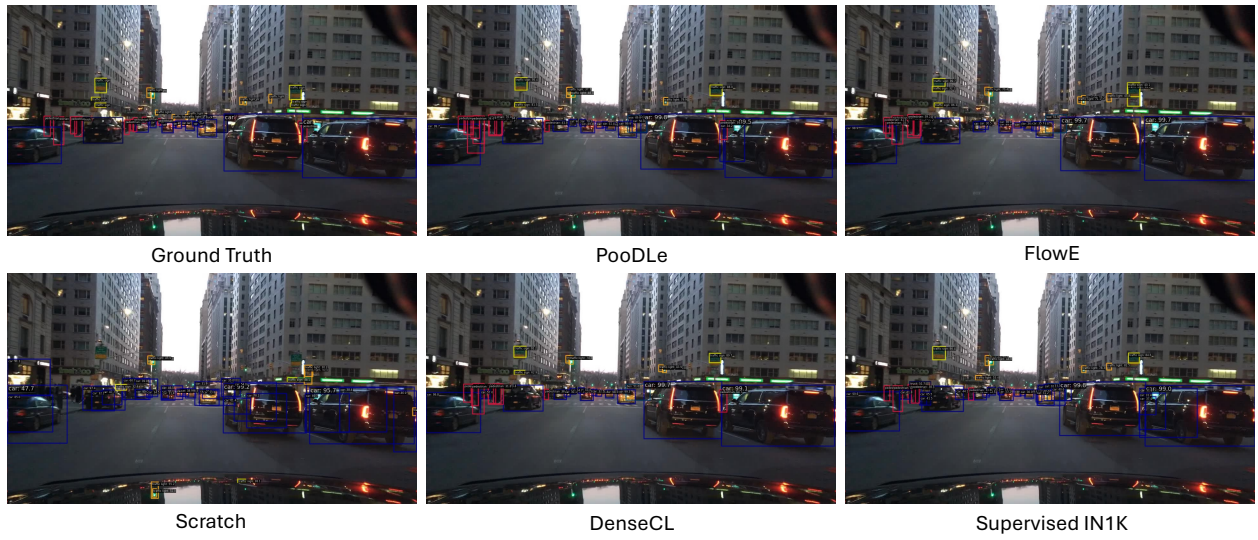


Figure 13: Visualizations of object detection bounding boxes for BDD FPN readout.

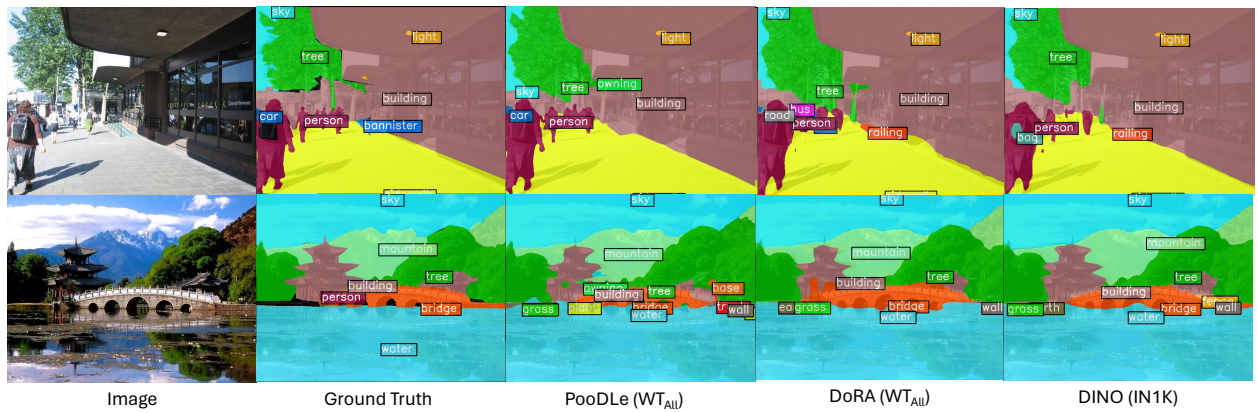


Figure 14: Visualizations of semantic segmentation masks for ADE UperNet finetuning.

E Additional evaluation results

Table 5: Additional BDD semantic segmentation (SemSeg) and object detection (Det) readout evaluations. All settings are conducted with a frozen backbone. † BYOL results are taken from FlowE [49] and used DeepLab v3 [9] in-place of Upernet [47]. *Pretrained on BDD, initialized with supervised ImageNet weights.

Method	Arch	Ep.	Pretrain	BDD100K Sem. Seg.				BDD100K Obj. Det.		Cityscapes Sem. Seg			
				Linear		UperNet		Det C4	FPN	Linear		UperNet	
				mIoU	Acc	mIoU	Acc	mAP	mAP	mIoU	Acc	mIoU	Acc
Scratch	R50	-	-	9.7	55.0	26.1	81.2	0.0	7.7	9.8	58.0	30.7	84.1
PooDLe	R50	100	BDD	39.2	89.2	49.9	91.8	4.9	25.2	47.2	90.2	60.7	93.5
Supervised	R50	600	IN1K	36.7	84.7	55.2	92.0	3.6	24.9	46.8	87.4	63.4	93.7
BYOL [20]†	R50	1000	IN1K	28.3	-	52.4	-	2.8	26.0	39.9	-	60.3	-
DenseCL [45]	R50	200	IN1K	21.3	82.7	52.8	91.6	0.3	25.0	27.3	84.0	63.7	93.7
Supervised	ViT-S	300	IN1K	41.9	88.5	50.9	91.4	-	-	46.8	87.4	63.4	93.7
DINO [7]	ViT-S	800	IN1K	38.5	88.1	52.3	92.0	-	-	47.1	90.3	63.6	94.0
iBOT [54]	ViT-S	800	IN1K	44.4	89.6	54.2	92.2	-	-	52.1	91.5	65.3	94.3
PooDLe	R50	100	BDD*	44.7	90.7	54.1	92.7	3.9	28.0	52.0	91.5	65.1	94.4

We compare PooDLe against ImageNet-pretrained baselines in Table 5 and observe that PooDLe outperforms most baselines except iBOT and ImageNet supervised ViT. This result is encouraging, as pretraining on naturalistic video is more challenging due to spatial and class imbalance, yet is also a more realistic setting that enables the use of broader sets of usable data. Furthermore, we note that pretraining on class-balanced data such as ImageNet particularly benefits mIoU, which weighs all classes equally despite some classes only appearing in a tiny proportion of pixels in evaluation. Finally, PooDLe pretrained on BDD with weights initialized from the ImageNet supervised checkpoint surpasses all ImageNet-pretrained baselines on linear semantic segmentation.

F Per-class evaluation results

Table 6: IoU per class on BDD semantic segmentation linear readout.

Method	Pretrain	Rd	Sky	Bldg	Veg	Car	Bus	Fence	Truck	Wall	S-walk	Terrain	Train	Pole	Bicycle	Person	M-cycle	Tr. Sign	Rider	Tr. Light
DINO	BDD	88.6	93.0	72.3	77.3	73.7	0.8	11.7	5.3	5.1	38.5	37.5	0	8.1	0	19.6	0	13.4	0	17.7
DenseCL	BDD	82.0	88.2	68.3	72.6	63.0	0	1.5	0.5	0	17.7	7.2	0	0.3	0	0.1	0	1.1	0	9.4
DoRA	BDD	89.9	93.6	75.4	79.9	76.6	5.1	17.9	11.0	10.8	44.6	42.7	0	13.3	0.7	25.2	0	20.5	0	23.9
FlowE	BDD	90.6	92.9	75.8	79.6	80.8	32.9	23.5	22.7	15.3	45.7	32.4	0	12.9	11.8	28.7	4.1	15.9	0	12.1
PooDLe	BDD	91.3	93.5	77.0	80.4	81.7	34.0	29.4	24.3	17.2	49.6	38.1	0	24.3	18.0	35.2	2.9	26.6	0	21.2
Supv.	IN	79.8	88.8	70.0	77.2	72.6	24.9	21.8	14.4	7.2	18.4	31.8	0	22.8	36.8	40.2	19.5	31.8	8.2	31.2
PooDLe	IN+BDD	92.6	94.0	80.3	82.2	84.8	54.7	34.9	33.4	17.8	56.3	42.2	0	25.7	27.1	41.5	7.7	39.0	0.1	35.2

Table 7: Defined groupings and statistics of classes in the BDD semantic segmentation dataset. L=Large, S=Small, C=Common, R=Rare.

	Rd	Sky	Bldg	Veg	Car	Bus	Fence	Truck	Wall	S-walk	Terrain	Train	Pole	Bicycle	Person	M-cycle	Tr. Sign	Rider	Tr. Light
Avg Pix. % / Im.	22.0	18.2	15.0	14.4	8.4	3.7	3.4	3.2	3.1	3.1	2.8	2.1	1.0	0.8	0.7	0.6	0.5	0.4	0.4
Total % of Pix.	21.3	17.3	13.2	13.2	8.1	0.6	1.0	1.0	0.5	2.0	1.0	0.0	0.9	0.1	0.3	0.0	0.3	0.0	0.2
Total % of Im.	96.5	94.8	88.4	91.7	97.3	15.0	30.6	30.5	15.4	66.7	36.7	0.7	95.0	6.4	34.7	3.8	75.3	5.2	47.1
Size Grp.	L	L	L	L	L	L	L	L	L	L	L	L	S	S	S	S	S	S	S
Freq. Grp.	C	C	C	C	C	R	C	C	R	C	C	R	C	R	C	R	C	R	R

We provide a breakdown of IoU per class on BDD semantic segmentation linear readout in Table 6. In Table 7, we also provide dataset-level statistics for each class computed over the training split of 7,000 images in the BDD semantic segmentation dataset, namely average pixel percentage per image, total percentage of pixels over the dataset and total percentage of images that they appear in over the dataset. Size and frequency groupings are then independently defined using these statistics and used in Table 3. A class is considered ‘Large’ (L) if its average pixel percentage per image is $> 1\%$ and ‘Small’ (S) otherwise. Separately, we define a class as ‘Common’ (C) if the total percentage of images it appears in is $> 20\%$ and ‘Rare’ (R)

otherwise. Notably, PooDLe achieves significant gains on small classes such as ‘Pole’, ‘Bicycle’, ‘Traffic Sign’, ‘Traffic Light’. Methods trained on BDD underperform supervised IN1K on classes rare in BDD such as ‘Rider’, likely because IN1K offers both abundant and iconic images of these object categories.

G Spatial token collapse in vision transformers

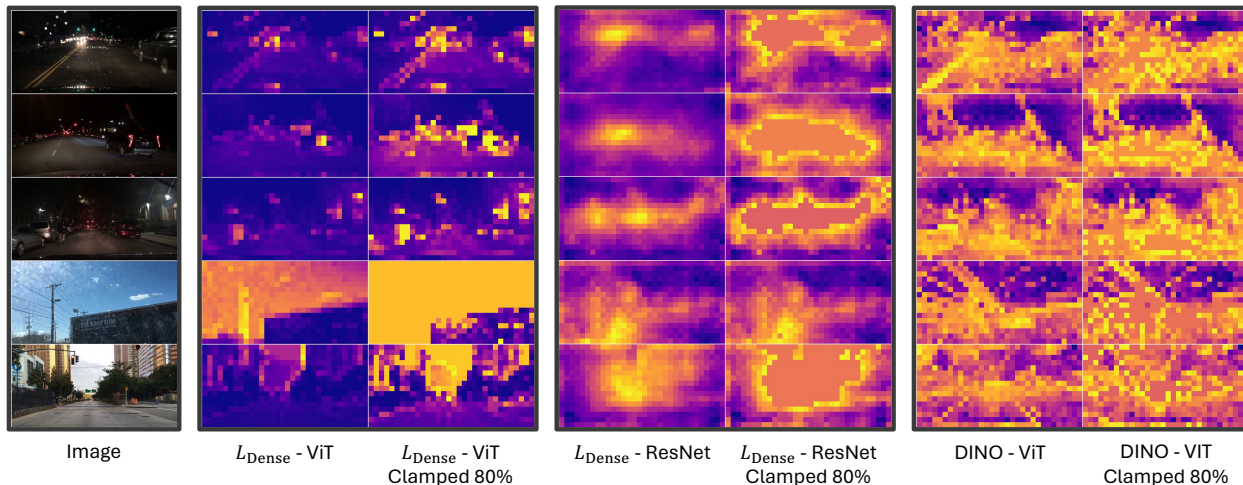


Figure 15: Comparison of L2 norm of last feature layer activations. The visualizations show both the raw L2 norm values as well as the L2 norm values clamped at the 80th percentile.

Initial attempts at using a ViT [16] backbone for PooDLe results in poor downstream performance. We hypothesize this is because of unwanted interaction between the model architecture and the FlowE dense objective. In our initial analysis, we have found that ViTs trained with only the FlowE dense objective results in background tokens receiving very high feature activations relative to other regions, as shown in Figure 15. This does not occur for our ResNet-based model as well as DINO-ViT which we believe is contributing to the performance drop. In the future, we would like to investigate this phenomenon further and formulate possible remedies to enable PooDLe to work with ViTs.

H Flow visualizations

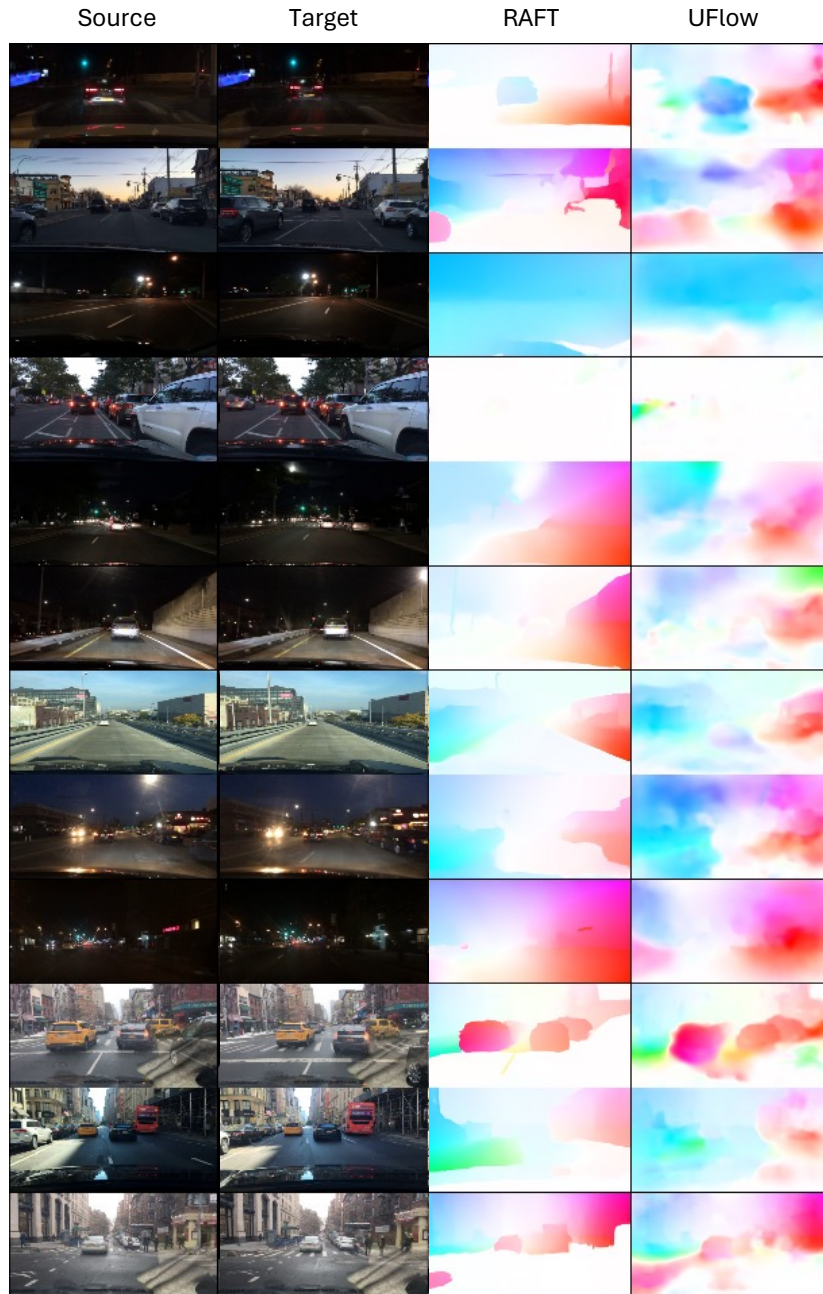


Figure 16: Comparison of predicted optical flow from RAFT (supervised) and UFlow (unsupervised)

In Figure 16, we compare the predicted flow maps generated from RAFT [40], an off-the-shelf supervised model, and our own unsupervised UFlow [30] model. The frame pairs are randomly sampled with $\Delta t \in [15, 30]$. We do note that self-supervised flow, particularly on BDD100K may exhibit noisy or splotchy results. This is possibly due to the inconsistent motion and large dark regions that do not offer sufficient photometric supervisory signal. This is in contrast to RAFT [40] which learns sharp edges like from supervised labels. Nevertheless, we find that this self-supervised flow is sufficient for training PooDLes.